# Nondestructive Identification of Colloidal Molecular Sieves Stabilized in Water

**B. Mihailova,[†] S. Mintova,*[,†] K. Karaghiosoff,[†] T. Metzger,[‡] and T. Bein[†]**

*Department of Chemistry, University of Munich, Butenandtstr. 11 (E), D-81377 Munich, Germany, and European Synchrotron Radiation Facility, ESRF, BP 220, Grenoble, France*

*Received: March 17, 2005; In Final Form: July 17, 2005*

The encapsulation of small quaternary ammonium ions in zeolite frameworks could be used as a base for investigation of the crystallization process of colloidal (nanosized) molecular sieves stabilized in water with Raman and $^{13}C$ NMR spectroscopic methods. The organic−framework interactions in colloidal microporous materials with LTA, FAU, BEA, and MFI topology have been considered; the results show that the crystallinity of nanosized particles with monomodal particle size distribution stabilized in water can be examined using the vibrational and magnetic resonance spectral features of the organic template molecules occluded in the specific pores and cages in the zeolite framework. The molecular packing effect and restricted mobility due to specific organic/framework interactions result in shifts and substantial broadening of the $^{13}C$ NMR signals, as well as in changes of the positions and the relative intensities of the Raman peaks. The spectroscopic methods are very efficient for analyzing the crystalline structures of nanosized molecular sieves stabilized in aqueous suspensions due to no restrictions related to the particle size.

## Introduction

The great industrial importance of zeolites as sorbents, catalysts, and ion exchangers as well as the possibility to tune their key macroproperties by varying the synthesis parameters provoke considerable scientific efforts into the design and structural characterization of novel microporous materials. The development of nanotechnologies and their requirements for synthesizing nanoscale multifunctional materials present new fascinating goals to modern solid-state chemistry of colloidal systems. Nanosized zeolite-type materials are of technological importance as building blocks for thin films and layers. To be utilized further, the nanosized zeolite crystals have to be stabilized in solvents such as water, ethanol, acetone, etc., with the solid concentration of the suspension commonly varying between 1 and 6 wt %. It is, therefore, of interest to develop efficient experimental methods for analyzing the structure of nanosized zeolite particles dispersed in colloidal suspensions. Zeolites have large unit cell parameters, up to 2.5 nm, thus the examination of nanocrystals sized below 10 nm, i.e., sized a few unit-cell repetitions, approaches the intrinsic limits of the X-ray diffraction method to detect a periodic atomic ordering. Transmission electron microscopy gives the opportunity to identify nanosized zeolite particles. However, one requires a careful purification of the colloidal particles and a stabilization of the sample to sustain the high-voltage electron beam for an adequate time of measurement.

Spectroscopy provides excellent tools for structure analysis of nanoparticles based on the different response to the incident radiation from characteristic atomic clusters distinguishable on a subnanometric scale. Among the various spectroscopic methods, Raman spectroscopy compares favorably with its ability to detect amorphous substance and to fingerprint different crystalline silica and alumosilicate materials.[1−4] Nanosized zeolites can be produced with or without organic templates (mostly quaternary ammonium salts) in the reaction mixture, but so far, only colloidal zeolites that are prepared with organic additives have a monomodal particle size distribution and can be further stabilized in appropriate solvents. Because of different atomic surroundings, the template molecules that are encapsulated in the zeolite structure differ in geometry (bond lengths, bond angles, conformations) from those in the initial synthesis mixture as well as from those trapped in the precursor amorphous substance. The changes in molecular geometry alter the vibrational modes of the organic molecules embedded in the zeolite skeleton,[5−9] thus making it possible to indicate the formation of zeolite structure via observed spectral changes in suitable Raman peaks arising from the organic template. These advantages, together with the fact that the Raman scattering cross section from organic molecules is very high, while water is a poor inelastic light scatterer, make Raman spectroscopy promising as a method for probing the structure of crystalline nanoparticles stabilized in water.

On the other hand, one should expect to distinguish the organic template molecules incorporated in the zeolite framework on the basis of their chemical shifts in the $^{13}C$ nuclear magnetic resonance (NMR) spectra. Solid-state NMR spectroscopic measurements performed on MFI- and sodalite-type zeolites have revealed the specific response of organic template molecules trapped in the inorganic host matrix.[10,11] Interestingly, the small crystallite size could allow applying liquid-state NMR spectroscopy for structural studies of colloidal zeolite suspensions based on the rapid Brownian motion of these particles in the solvent. Recently, it has been demonstrated that $^{29}Si$ liquid NMR spectroscopic measurements can be performed on nonpurified synthesis precursor solutions in order to follow the formation of the zeolite framework with MEL framework topology.[12]

Herein we report on nondestructive identification of nanosized zeolite particles stabilized in water using the Raman and/or $^{13}C$ NMR spectral features of the organic template molecules

* Author to whom correspondence should be addressed. E-mail: svetlana.mintova@cup.uni-muenchen.de. Fax: +4989 2180 77622.
[†] University of Munich.
[‡] European Synchrotron Radiation Facility.

10.1021/jp051413v CCC: $30.25 
Published on Web 08/20/2005

encapsulated in the zeolite skeleton. The utilization of Raman and $^{13}C$ NMR spectra of the organic templates for examination of the structure of the corresponding colloidal zeolite can be suitable because of the following reasons: (i) there are no restrictions due to the small size of the crystalline domains, which allows probing of the structure of very small particles; (ii) the intense spectroscopic signals from the organic molecules ensure the sufficient sensitivity of the method even in the case of low concentrations of the colloidal suspension; and (iii) stabilized colloidal zeolites with narrow particle size distribution always contain organic molecules, which suggests wide applicability of the approach. We present our results for four types of microporous materials of technological importance: LTA, FAU, BEA, and MFI.

## Experimental Section

The nanosized zeolite crystals were synthesized from clear precursor solutions containing organic templates: tetramethylammonium hydroxide ($TMA{\cdot}5H_2O$) in the case of zeolites A (LTA type structure) and Y (FAU type structure), tetraethylammonium hydroxide (TEAOH, 20 wt %) in the case of zeolite Beta (BEA type structure), and tetrapropylammonium hydroxide (TPAOH, 1.0 M in $H_2O$) in the case of silicalite-1 (MFI type structure). The synthesis procedure is described in detail in refs 13−16. The crystalline nanoparticles were extracted from the reaction mixture by a three-step centrifugation (20 000 rpm for 180 min) and a subsequent redispersion in doubly distilled water, thus achieving stabilized zeolite suspensions in water with a pH value ranging from 8.5 to 10 and concentrations between 1.5 and 10 wt %.

The average particle size was determined by dynamic light scattering (ALV−NIBS/HPPS). The crystalline habit and the atomic network periodicity of the nanoparticles were probed by high-resolution transmission electron microscopy (Philips 200 FEG TEM). The crystallinity of the zeolite powder samples that were used as reference probes was verified by powder X-ray diffraction (Scintag XDS 2000). Additional study of the zeolite suspensions containing MFI nanoparticles with sizes in the range of 10−20 nm was carried out at beamline ID01, ESRF, Grenoble, using a six-circle diffractometer equipped with a position- sensitive detector.

The Raman spectra were measured at room temperature with a Bruker Equinox 55 FT-IR spectrometer equipped with an FRA106/S FT-Raman module, a liquid $N_2$ cooled Ge detector, and an Nd:YAG laser operating at 1064 nm. The spectra were collected in backscattering geometry using a standard one-side mirrored quartz-glass suprasil cuvette (Hellma QS 0.500) for the liquid samples. The acquisition of each spectrum was performed with an output laser power of 500 mW, spectral resolution of 4 $cm^{-1}$, and by averaging 3600 scans (approximately 2 h accumulation time). The as-measured spectra of the water-stabilized colloidal zeolite samples were subtracted by the spectrum of water recorded under the same experimental conditions in order to eliminate the contribution of both water and the silica-glass cell.

The absence of amorphous substance in the reference samples was additionally checked by measuring the Raman spectra of the calcined samples (450 °C for 8 h).

The $^{13}C$ NMR spectra of the liquid samples were collected with a JEOL Eclipse 400 NMR spectrometer operating at 100.6 MHz. The experiments were carried out in 5-mm glass tubes at 25 °C with broadband proton decoupling. The spectra were recorded after the averaging of 25 000 scans using the 30° pulse and a relaxation delay of 0.5 s, resulting in a repetition time of 2 s and a total accumulation time of about 14 h. Line broadening (10 Hz) and zero filling, resulting in a final digital resolution of 0.4 Hz per data point, were applied to every FID prior to Fourier transformation. The solid-state $^{13}C$ MAS NMR measurements of the reference powder samples were performed with 4-mm $ZrO_2$ rotors using a DSX advance impulse spectrometer (Bruker DSX Avance 500) operating at a resonance frequency of 125 MHz; all spectra were recorded at a spinning rate of 12 kHz. Cross-polarization (8 ms contact time) and high-power proton decoupling (TPPM pulse sequence, 70 kHz decoupling power) was applied during the collection of all spectra.

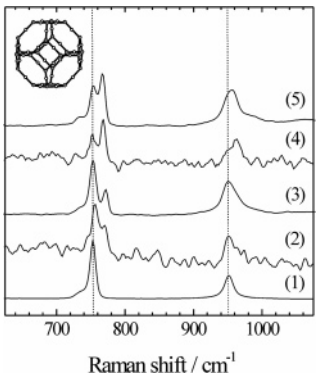


**Figure 1.** Raman spectra of: (1) TMAOH 25 wt % in $H_2O$, (2) 2.1 wt % aqueous suspension of 50-nm-sized zeolite Y, (3) freeze-dried powder of as-synthesized zeolite Y, (4) 2.2 wt % aqueous suspension of 40-nm-sized zeolite A, and (5) freeze-dried powder of as-synthesized zeolite A. The dashed lines trace the positions of the peaks in the spectrum of TMAOH that originate from N−C bond stretching modes. The inset represents a sodalite cage, the building unit of the two zeolite structures.

## Results and Discussion

**TMA-Containing LTA and FAU Suspensions**. Zeolites with LTA and FAU framework topologies are crystalline alumosilicates containing sodalite cages linked via double four- and six-membered rings, respectively, thus forming different three-dimensional pore systems. The colloid form of both LTA- and FAU-type zeolites is prepared by adding tetramethylammonium (TMA) ions as an organic template to the synthesis solution.[13,17] The TMA ions are incorporated in the sodalite cages as well as in the channels of the zeolite skeleton. The TMA ions embedded in the sodalite cages are under a strong elastic stress along the direction of the C−N bonds because of the similar size of the cation and the cage inner space (~6.5 Å). As a result, the symmetrical and antisymmetrical $NC_4$ stretching modes of TMA occluded in sodalite cages shift to higher energies and generate Raman peaks positioned at wavenumbers higher that those of TMA in an aqueous solution, the effect being more pronounced for the symmetrical mode.[5−7]

The Raman spectra of a series of colloidal zeolite suspensions with different concentrations and particle size were measured and compared with the spectra of free TMA ions and of the freeze-dried zeolite samples. The Raman spectra of TMA in water, of colloidal zeolite suspensions, and of the corresponding powder reference samples of zeolites Y and A are presented in Figure 1. The Raman scattering in the range 730−770 and 930−980 $cm^{-1}$ is generated from the symmetrical and antisymmetrical $NC_4$ stretching modes, respectively. The TMA species trapped in the precursor amorphous solidified substance during the crystallization of LTA and FAU-type zeolites exhibited the same Raman spectra as that of TMA in water solution. The Raman signals generated by the N−C stretching are positioned at 753

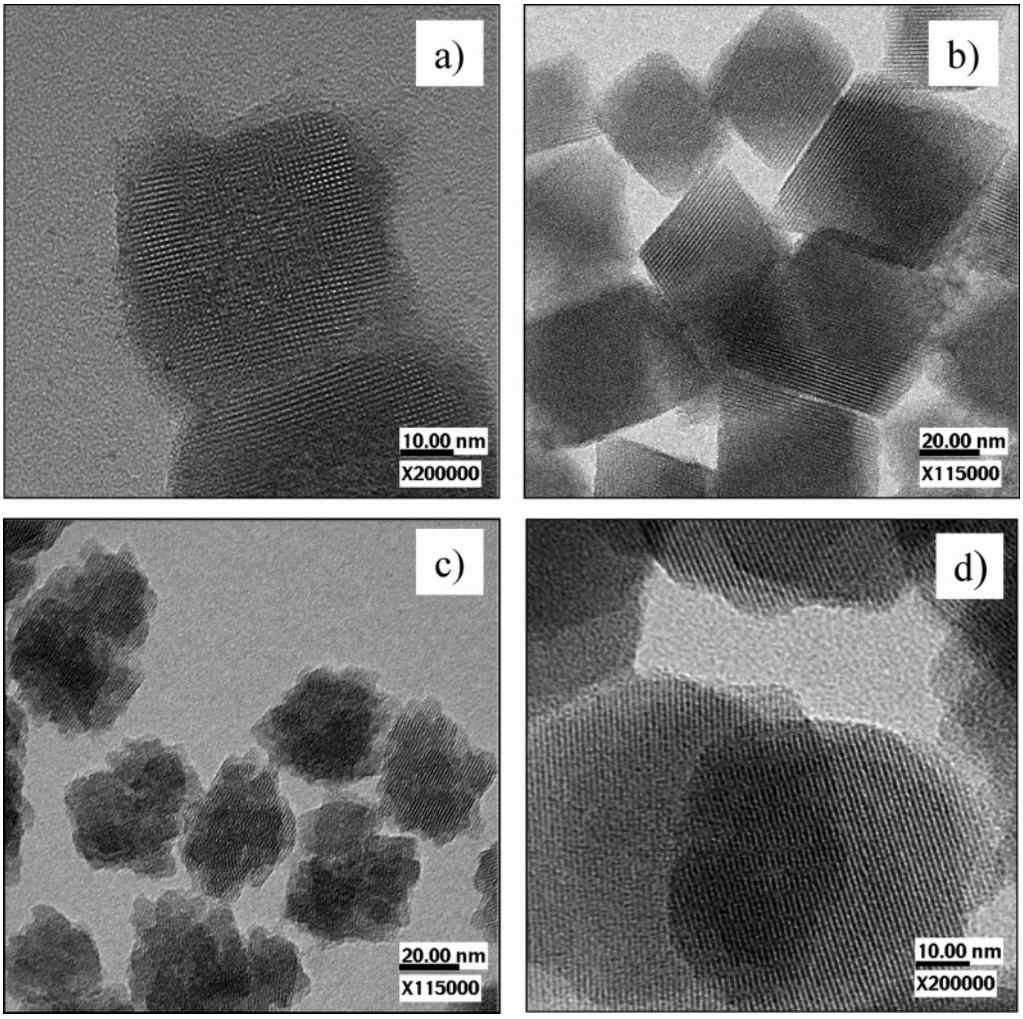


**Figure 2.** HRTEM images of (a) zeolite A, (b) zeolite Y, (c) zeolite Beta, and (d) silicalite-1.

and 951 $cm^{-1}$. The appearance of additional, higher-energy-shifted Raman scattering at about 770 and 960 $cm^{-1}$ is a strong indication for the formation of crystalline sodalite-type zeolite structure. Hence, zeolite Y may be distinguished from zeolite A through the position of the additional Raman peak arising from the symmetrical C−N bond-stretching mode. Because of the smaller size of the sodalite cages in zeolite Y compared to zeolite A, the Raman signal generated by the sodalite-cage-trapped TMA ions appears at 772 $cm^{-1}$ for zeolite Y, while for zeolite A, it appears at 767 $cm^{-1}$. In addition, the intensity ratio $\rho$ between the peaks at about 755 and 770 $cm^{-1}$ is larger than unity for zeolite Y and lower than unity for zeolite A because of the different relative amounts of TMA embedded in the sodalite cages. For the same reason, the band originating from the antisymmetrical C−N bond stretching modes appears blue-shifted for zeolite A (positioned at 958 $cm^{-1}$), while only a high-energy tail of the band is observed for zeolite Y.

One should note that the relative amount of sodalite-cage-trapped TMA ions varies with the Si/Al ratio within the same zeolite topology, thus reflecting on the relative Raman intensities. However, without doubt, the appearance of an additional peak near 770 $cm^{-1}$ is an indicator for the existence of sodalite-phase zeolite crystals. As seen in Figure 1, the spectra of colloidal zeolite Y (curve 2) and zeolite A (curve 4) stabilized in water exhibit the same spectral pattern as the spectra of powder samples. For zeolite Y, the additional peak at 772 $cm^{-1}$ is clearly seen, and the asymmetrical broadening (change in the higher-energy slope) of the band at 951 $cm^{-1}$ can also be noticed. For zeolite A, the additional peak at 767 $cm^{-1}$ and the blue-shift of the band near 950 $cm^{-1}$ are well pronounced. These spectral features were recorded for aqueous solutions, with zeolite concentration varying from 1.5 to 3.5 wt %. The average size of the zeolite particles is 40 nm for zeolite A and 50 nm for zeolite Y, as estimated from dynamic light scattering measurements and by TEM (see Figure 2 a,b). The HRTEM images reveal also the specific crystallite habit: an approximately cubic particle shape for zeolite A and an octahedral for zeolite Y.

The reference solid-state $^{13}C$ NMR spectra of $TMAOH{\cdot}5H_2O$ and of zeolites Y and A are shown in Figure 3a. Similar to the results of the Raman study of the C−N vibration modes, the pure TMA produces only one $^{13}C$ NMR signal positioned at 57.5 ppm, while two peaks at 56.5 and 58.5 ppm are observed for TMA embedded in the zeolite structure. The larger $^{13}C$ chemical shift corresponds to TMA trapped in the sodalite cage, while the smaller $^{13}C$ chemical shift corresponds to TMA in the larger zeolite pores.[9] In addition, the full width at the half-maximum (fwhm) of the NMR peaks in the spectra of zeolites is larger than that in the spectrum of pure TMA, most probably due to the influence of the zeolite skeleton atoms on the organic template atoms and the greater distribution in the local atomic environment of carbon. The liquid-state $^{13}C$ NMR spectra of TMA in water, and of colloidal zeolites Y and A stabilized in water, are presented in Figure 3b. All the spectral features observed by solid-state NMR are also detected by liquid-state NMR spectroscopy. Two carbon chemical shifts are observed

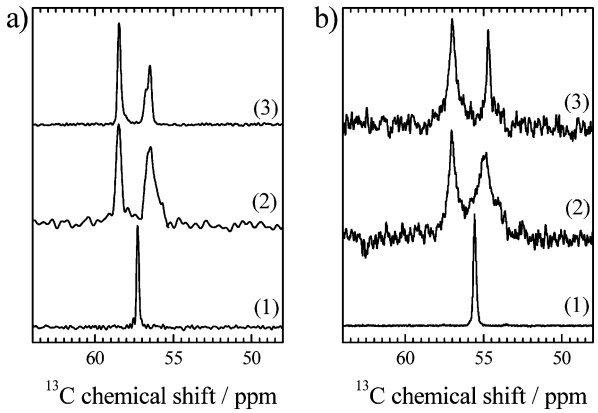


**Figure 3.** (a): Solid-state $^{13}$C NMR spectra of: (1) pure TMAOH·5$H_2O$, (2) freeze-dried as-synthesized zeolite Y, and (3) freeze-dried as-synthesized zeolite A. (b): Liquid-state $^{13}$C NMR spectra of (1) TMAOH 25 wt % in $H_2O$, (2) 2.1 wt % aqueous suspension of 50-nm-sized zeolite Y, and (3) 2.2 wt % aqueous suspension of 40-nm-sized zeolite A.

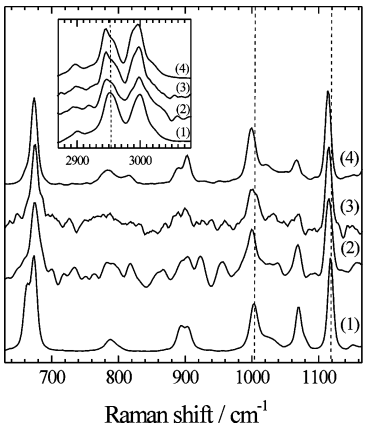


**Figure 4.** Raman spectra of: (1) TEAOH 20 wt % in $H_2O$, (2) 2.8 wt % aqueous suspension of 30-nm-sized zeolite Beta, (3) 10 wt % aqueous suspension of 30-nm-sized zeolite Beta, and (4) freeze-dried as-synthesized zeolite Beta. The inset displays the spectral range generated by the C−H bond stretching vibrations. The dashed lines trace the positions of the peaks in the spectrum of TEAOH that have the most pronounced red-shift.

in the spectra collected from the colloidal zeolite suspensions instead of one as in the spectrum of free TMA ions; the two peaks are positioned at up- and downfield compared to the signal of free $TMA^+$. Moreover, the $^{13}$C NMR signals in the spectra of the colloidal zeolite are broader than that in the spectrum of TMA. The peak positions measured by liquid- and solid-state NMR spectroscopy differ only slightly from each other. This overall chemical shift change may result from differences in magnetic susceptibility between solid and liquid media. Two $^{13}$C NMR signals have also been observed in other zeolites containing $TMA^+$ encapsulated in the sodalite cage.[10] Likewise, we attribute the peak at 57.0 ppm observed in the liquid-state $^{13}$C NMR spectra to $TPA^+$ species embedded into the sodalite cages, while the signal near 55.0 ppm is assigned to $TMA^+$ incorporated into the channels and/or the supercage (for FAU framework). Therefore, by using liquid-state $^{13}$C NMR spectroscopy, the presence of sodalite-type zeolite crystallites in aqueous suspensions can be detected via: (i) existence of an additional peak positioned at higher ppm values than that of free $TMA^+$ and (ii) increase of the peak width. It is worth noting that the ratio between the integrated intensities of the peaks near 55.0 and 57.0 ppm is larger for zeolite Y than for zeolite A, which is in good accordance with the Raman spectroscopic data, revealing different relative amounts of $TMA^+$ occluded in the sodalite cages in the two types of zeolites.

**TEA-Containing BEA Suspensions.** Another type of zeolite with a great potential as a catalyst is zeolite Beta (BEA framework topology). This zeolite belongs to the family of disordered zeolite structures and has a high degree of stacking disorder along the tetragonal *c*-axis.[18] The existence of faults in the layer connectivity results in a nonregular shape of the zeolite Beta nanoparticles, although they exhibit clearly atomic long-range ordering (see the HRTEM image in Figure 2c). The structure of the ordered end-members possesses a three-dimensional pore system with two types of openings, sized about 6.4 Å × 7.6 Å and 5.5 Å × 5.5 Å. The synthesis of zeolite Beta nanocrystals is strongly facilitated if tetraethylammonium (TEA) hydroxide is used as an organic template. The size of $(C_2H_5)_4N^+$ is estimated at ca. 6.5−7.5 Å.[19] Therefore, as in the case of TMA trapped in sodalite cages, one should expect a blue-shift of the Raman peaks generated by the C−C−N stretching modes. In fact, such spectral differences between TEA in water and occluded in zeolite Beta are observed in the range 640−930 cm$^{-1}$ (see Figure 4, curves 1 and 4): (i) one peak at 674 cm$^{-1}$ in the spectrum of TEA trapped in the BEA framework instead of two peaks at 664 and 674 cm$^{-1}$ for free TEA ions, (ii) the appearance of Raman scattering near 810 cm$^{-1}$, in addition to the peak at 786 cm$^{-1}$, and (iii) an increase in the intensity ratio between the peaks at 903 and 890 cm$^{-1}$. The last two features are very similar to those observed for TMA. Most probably, the Raman scattering at 780−810 and 890 cm$^{-1}$ arises from the symmetrical and asymmetrical C−N bond stretching modes of TEA, respectively, while the Raman scattering in the range 660−680 cm$^{-1}$ is generated by stretching modes of the whole C−C−N chain. Therefore, the main reason for the observed spectral changes in the range 640−930 cm$^{-1}$ is the elastic stress of TEA along the C−C−N chains due to the confined space for this ion in the pores of zeolite Beta. One should mention that Raman-active phonons of the zeolite Beta framework might also contribute to the additional Raman scattering near 810 cm$^{-1}$, as revealed by the spectra of TEA-free samples. Further, there is a detectible red-shift of the peaks at 1003 and 1117 cm$^{-1}$, related to $CH_2$ modes, as well as splitting and a red-shift of the more intense component of the band at 2952 cm$^{-1}$, which originates from a C−H bond-stretching mode. These lower-energy shifts are due to the interactions of the H atoms from TEA with the surrounding framework atoms. The Raman spectrum of TEA trapped in the noncrystalline solidified precursor material is the same as that of TEA in water. Thus the above-discussed spectral features can be used for fingerprinting the zeolite Beta structure. However, the Raman scattering from C−N bond stretching is not intense, and even for zeolite suspensions of high concentration, it is masked by the noise (see Figure 4, curves 2 and 3). Therefore, the most appropriate Raman spectroscopic features for detecting zeolite Beta nanocrystallites are: (i) existence of a single peak at 674 cm$^{-1}$ instead of two signals at 664 and 674 cm$^{-1}$, (ii) red-shift of the peaks at 1004−999 cm$^{-1}$ and of the peak at 1118−1113 cm$^{-1}$, and (iii) splitting of the band at 2952 cm$^{-1}$ and red-shift of the more intense component to 2945 cm$^{-1}$.

The $^{13}$C NMR spectra of TEA ions in aqueous solution and embedded in the zeolite Beta structure are depicted in Figure 5. The two signals observed at 51.8 and 6.1 ppm for the aqueous solution of TEA correspond to the methylene and methyl carbon atoms, respectively. When TEA is incorporated in the structure of zeolite Beta, the two peaks shift slightly to lower field and strongly broaden, the peak width being enlarged from ∼15 Hz

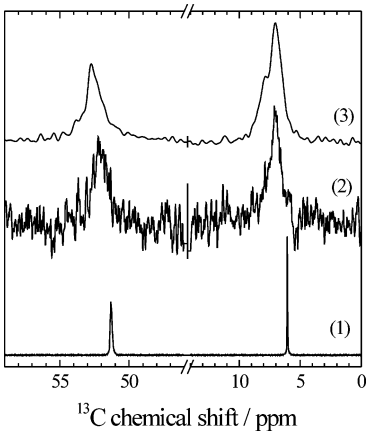


**Figure 5.** $^{13}$C NMR spectra of: (1) TEAOH 20 wt % in $H_2O$, (2) 2.8 wt % aqueous suspension of 30-nm-sized zeolite Beta, and (3) freeze-dried as-synthesized zeolite Beta.

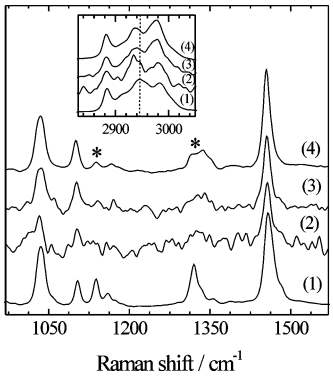


**Figure 6.** Raman spectra of: (1) TPAOH 1.0 M in $H_2O$, (2) 1.5 wt % aqueous suspension of 20-nm-sized silicalite-1-type particles, (3) 3.0 wt % aqueous suspension of 50-nm-sized silicalite-1, and (4) freeze-dried 50-nm-sized silicalite-1. The asterisks mark the Raman bands, whose relative intensity is most sensitive to existence of TPA conformations typical of MFI structure; the line traces the position of the C−H bond stretching peak in the spectrum of TPAOH having the most pronounced red-shift due to the embedding of TPA in the MFI structure.

to ∼120 Hz (see Figure 5). The large width of the NMR signals could indicate molecular packing effects and restricted mobility due to specific organic/framework interactions, as deduced from the Raman spectroscopic data. The same features are observed in the $^{13}$C NMR spectra collected from the powder sample of zeolite Beta and from the colloidal zeolite Beta suspension. Therefore, by applying liquid-state $^{13}$C NMR spectroscopy, one can identify zeolite Beta nanocrystals stabilized in water through the increase in the fwhm of the observed peaks in comparison with the peaks of pure organic molecules.

**TPA-Containing MFI Suspensions.** The applicability of Raman and liquid-state $^{13}$C NMR spectroscopy for structure control of colloidal zeolite suspensions was also verified on silicalite-1 particles sized 50 nm (see Figure 2d). Silicalite-1 is of MFI-type framework topology and, in colloidal form, is synthesized with tetrapropylamonium (TPA) cations as a structure-directing template. The Raman spectra of the nanoparticles stabilized in water exhibit the spectral features typical of the TPA species that adapt to the pore structure of MFI (see Figure 6): red-shift of the C−H stretching mode from 2954 to 2937 cm$^{-1}$ and splitting and change in the relative intensity of the $CH_2$ modes in the range 1130−1370 cm$^{-1}$.[5,8] The repeatability of the results was checked for suspensions with concentrations varying from 1.5 to 6.0 wt % and for particles sized 50 and 20 nm. In the range of C−H stretching modes, the spectral

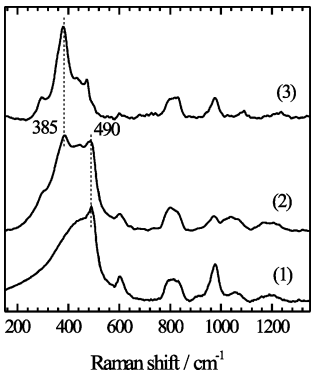


**Figure 7.** Raman spectra of calcined: (1) initial sample extracted from precursor solution aged for 24 h, (2) 20-nm-sized silicalite-1-type particles obtained after 30 days aging of precursor solution,[16] and (3) 50-nm-sized silicalite-1 particles. Raman signals at 385 and 490 cm$^{-1}$ are typical of MFI-type framework and noncrystalline silica, respectively.

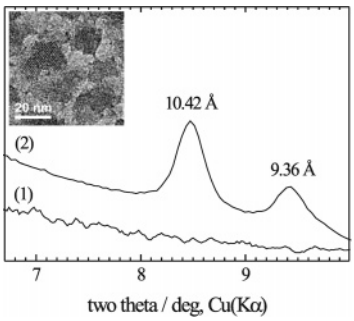


**Figure 8.** XRD patterns of powdered sample of 20-nm-sized silicalite-1 measured (1): by a laboratory diffractometer (Cu Kα radiation) and (2) at ESRF, Grenoble (probe-radiation energy $E = 16$ keV). The insert shows the TEM image of the sample.

profile of the 20-nm-sized particles is not exactly the same as that of the 50-nm-sized particles; a lower-energy shift of the peak at 2954 cm$^{-1}$ is noticeable, and the relative intensities of the peaks do not resemble those of well-crystalline MFI structure. This observation can be explained by the presence of noncrystalline substance, i.e., a lower degree of crystallinity of the sample composed of 20-nm-sized particles. The latter assumption was confirmed by the Raman spectra of the calcined samples, revealing coexistence of a crystalline phase of MFI-type and amorphous silica (Figure 7). It is worth noting that the presence of long-range ordering in the powdered sample of 20-nm size was detected by XRD only when synchrotron radiation was used (Figure 8). The pattern shown in Figure 8b exhibits the Bragg reflections typical of MFI framework topology. In addition, the average size of the crystalline particles was determined using the Scherer equation based on the XRD patterns; the size of the crystalline domains is ∼23 nm, which is in a good agreement with TEM imaging observation.

The $^{13}$C NMR spectra of 50-nm-sized silicalite-1 in aqueous suspension and in a powdered form are shown in Figure 9. The spectrum of TPAOH in a water solution is also given for comparison. Similar to the case of zeolite Beta, a large broadening of the signals occurs when the TPA cations are incorporated in the MFI framework. The signal at 10.3 ppm generated by the methyl carbon splits into two components, which are associated with $CH_3$ groups located in the two different types of the MFI channels.[20] The liquid-state $^{13}$C NMR spectrum exhibits lesser signal-to-noise ratio and poorer spectral resolution than the solid-state spectrum. Yet the broadening of the $^{13}$C NMR signals as a result of the embedding of TPA into the particle bulk is clearly seen. Therefore, MFI-type zeolite

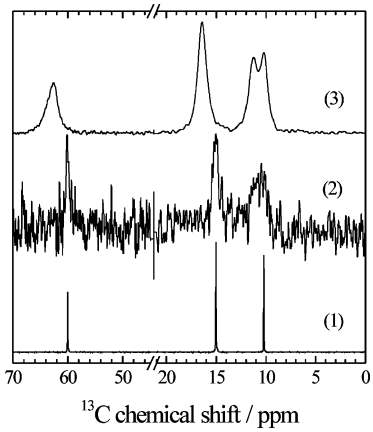


**Figure 9.** $^{13}C$ NMR spectra of: (1) TPAOH 1.0 M in $H_2O$, (2) 3.0 wt % aqueous suspension of 50-nm-sized silicalite-1, and (3) freeze-dried as-synthesized silicalite-1.

nanoparticles stabilized in water can be identified mainly on the basis of the strongly enlarged peak widths, especially in the range near 11 ppm.

## Conclusion

In conclusion, the changes in the geometry and the atomic surroundings of the organic template molecules occluded in the specific pores and cages of the zeolite framework provide an excellent opportunity to use Raman scattering and liquid-state $^{13}C$ nuclear magnetic resonance for detecting the existence of crystalline domains in nanosized zeolites stabilized in water. Raman scattering compares favorably to liquid-state $^{13}C$ NMR due to the shorter time of measurement, easier handling of the experimental setup, and the potential to allow a more precise distinction between precursor amorphous and crystalline zeolite nanoparticles. On the other hand, liquid-state $^{13}C$ NMR spectroscopy can also be applied to characterize colloidal zeolite particles stabilized in various solvents. Therefore, depending on the corresponding needs, one can preferably utilize the Raman or the liquid-state NMR analysis for nondestructive probing of the structure of the zeolite nanoparticles stabilized in solvents. Our study reveals also that colloidal systems with particle sizes that approach the size of giant molecules can be successfully investigated by liquid-state NMR spectroscopy. The present paper reports mainly on two approaches for measurements of colloidal zeolite crystals stabilized in solutions that could be applied further for preparation of two- and three-dimensional films and constructs used without the necessity of drying the samples prior to their characterizations.

**Acknowledgment.** The financial support of the DFG-CNRS bilateral program and PROCOPE is gratefully acknowledged. The authors thank Dr. J. Senker for measuring the solid-state NMR spectra and Dr. N. H. Olson for the acquisition of the TEM images.

## References and Notes

(1) Dutta, P. K.; Rao, K. M.; Park, J. Y. *J. Phys. Chem.* **1991**, *95*, 6654.
(2) Kingma, K. J.; Hemley, R. J. *Am. Mineral.* **1994**, *79*, 2969.
(3) Pasquarello, A.; Car, R. *Phys. Rev. Lett.* **1998**, *80*, 5145.
(4) Yu, Y.; Xiong, G.; Li, C.; Xiao, F.-S. *Microporous Mesoporous Mater.* **2001**, *46*, 23.
(5) Dutta, P. K.; Puri, M. *J. Phys. Chem.* **1987**, *91*, 4329.
(6) Dutta, P. K.; Del Barco, B.; Shieh, D. C. *Chem. Phys. Lett.* **1986**, *127*, 200.
(7) Hong, S. B. *Microporous Mater.* **1995**, *4*, 309.
(8) Li, Q.; Mihailova, B.; Creaser, D.; Sterte, J. *Microporous Mesoporous Materials* **2001**, *43*, 51.
(9) Ashtekar, S.; Barrie, P. J.; Hargreaves, M.; Gladden, L. F. *Angew. Chem., Int. Ed. Engl.* **1997**, *36*, 876.
(10) Jarman, R. H.; Melchior, M. T. *J. Chem. Soc., Chem. Commun.* **1984**, 414.
(11) Kovalakova, M.; Wouters, B. H.; Grobet, P. J. *Microporous Mesoporous Mater.* **1998**, *22*, 193.
(12) Mintova, S.; Petkov, N.; Karaghiosoff, K.; Bein, T. *Microporous Mesoporous Mater.* **2001**, *50*, 121.
(13) Mintova, S.; Olson, N.; Valtchev, V.; Bein, T. *Science* **1999**, *283*, 958.
(14) Mintova, S.; Olson, N.; Bein, T. *Angew. Chem., Int. Ed.* **1999**, *38*, 3201.
(15) Schoeman, B. J.; Babouchkina, E.; Mintova, S.; Valtchev, V.; Sterte, J. *J. Porous Mater.* **2001**, *8*, 13.
(16) Mintova, S.; Olson, N. H.; Senker, J.; Bein, T. *Angew. Chem., Int. Ed.* **2002**, *41*, 2558.
(17) Holmberg, B. A.; Wang, H.; Norbeck, J. M.; Yan, Y. *Microporous Mesoporous Mater.* **2003**, *59*, 13.
(18) Newsam, J. M.; Treacy, M. M. J.; Koetsier W. T.; de Gruyter, C. B. *Proc. R. Soc. London A* **1988**, *420*, 375.
(19) Szostak, R. *Molecular Sieves: Principles of Synthesis and Identification*; Blackie Academic & Professional: London, 1998.
(20) Millini, R.; Perego, G.; Berti, D.; Parker, W. O., Jr.; Carati, A.; Bellussi, G. *Microporous Mesoporous Mater.* **2000**, *35*−*36*, 387.